Off-resonance-enhanced polarization control in two-color atomic ionization

D. I. R. Boll,[1,*] L. Martini,[2] O. A. Fojón,[2] and A. Palacios[1,3]
[1]*Departamento de Química, Modulo 13, Universidad Autónoma de Madrid (UAM), 28049 Madrid, Spain*
[2]*Instituto de Física Rosario, CONICET-UNR, Blvd. 27 de Febrero 210 bis, 2000 Rosario, Argentina*
[3]*Institute of Advanced Research in Chemical Sciences (IAdChem), UAM, 28049 Madrid, Spain*

(Received 10 September 2019; published 21 January 2020)

We investigate a polarization control scheme in two-color two-photon atomic ionization. Experiments employing free-electron laser or high-order harmonic generation sources have shown light polarization dependencies in above threshold ionization of atoms assisted with an IR field. These were mostly performed at relatively high photoelectron energies where the soft-photon approximation remains valid. We use here a perturbation theory approach to show the larger degree of control that can be attained when the short wavelength photon energy is below the ionization threshold. This largely unexplored energy region offers unique possibilities to achieve polarization control of the reaction.

DOI: 10.1103/PhysRevA.101.013428

The investigation of nonlinear processes in excitation and ionization of gas phase experiments has been revitalized with the novel capabilities offered by Free Electron Laser (FEL) facilities [1,2]. The high spectral resolution, together with a fine-tunability in frequency and light polarization state, achieved by FELs enable the possibility of exploring new control schemes combining two-color fields [3–5]. For instance, time-resolved two-color multiphoton experiments in atoms have been realized at FERMI capturing the time-varying photoelectron angular distributions as a result of the interferences between one and two-photon absorption paths [4,5]. A conceptually different approach to steer the relative contributions of photoionization channels with different angular momenta is that of polarization control. In this scheme, the relative polarization angle between the fields is modified, giving rise to dichroic effects [6]. An equivalent strategy was previously employed to study the resonance-enhanced two-photon ionization of atomic targets where a weak synchrotron source was used in combination with a continuous laser beam [7].

Very recent experiments performed at the Linac Coherent Light Source (LCLS) have shown the high polarization tunability in x-ray beams, also controlling the photoelectron angular distributions by varying the time delay in x-ray two-color, two-polarization scheme [8]. These experiments followed a series of existing two-color experiments performed at the Free electron LASer in Hamburg (FLASH) combining extreme ultraviolet long pulses with optical or IR fields to investigate the polarization dependencies in an above-threshold ionization process in rare gases [3,9]. Briefly, the single-photon ionization (pump) of atomic and molecular targets by EUV light pulses gives rise to a photoelectron distribution in the continuum. The additional exchange of photons with the IR light source (probe) generates a sequence of secondary photoelectron peaks called sidebands. In order to avoid contributions from different paths and/or the parity mixing due to spectral overlap, nearly monochromatic EUV pulses lasting tens of femtoseconds were employed. These experimental results captured a modulation in the sideband signal as a function of the relative polarization angle between the interacting laser fields as plotted in Fig. 1. We here demonstrate that it is indeed possible to achieve a larger degree of control over the photoionization signal in the energy region where off-resonance below-threshold ionization occurs.

Figure 1 illustrates the control scheme recently employed at FLASH to explore dichroic effects in two-color above-threshold ionization (ATI) of atoms [3,9]. The intensity of the sideband, resulting from the combined absorption of an EUV and an IR photon, varies with the relative polarization state of the fields. As expected, the absorption of an IR photon from the ground state and subsequent absorption of an EUV to promote the electron to the continuum, i.e., two-photon path B in Fig. 1 (left panel), has a negligible contribution. The maximum ionization signal, as shown in the right panel of the same figure, is obtained for a collinear arrangement of the fields, while the minimum corresponds to cross-polarized fields. Because the photoelectron energy is significantly larger than that of the dressing IR field, the experimental data could be explained in terms of the soft-photon approximation [9,10]. This approximation, however, breaks down as the photoelectron energy decreases, and a second-order perturbation theory (SOPT) formalism (full line in Fig. 1) is required to accurately reproduce the ionization signal. This intensity modulation [11] can be defined as $\Delta = (\sigma_{\parallel} - \sigma_{\perp})/\sigma_{\parallel}$, where $\sigma_{\parallel(\perp)}$ is the total ionization probability for a parallel (perpendicular) polarization between the fields. It can then be retrieved as a function of EUV photon frequency, or equivalently the photoelectron energy. In Fig. 2(b), we show the experimental results obtained in the helium atom irradiated with an IR dressing field of 800 nm combined with XUV pulses generated at FLASH by Meyer *et al.* [9] (circles) and by generating the XUV pulse in a high-order harmonics experiment [12] (square with error bar). Experimental results from [13] using

*diego.boll@uam.es

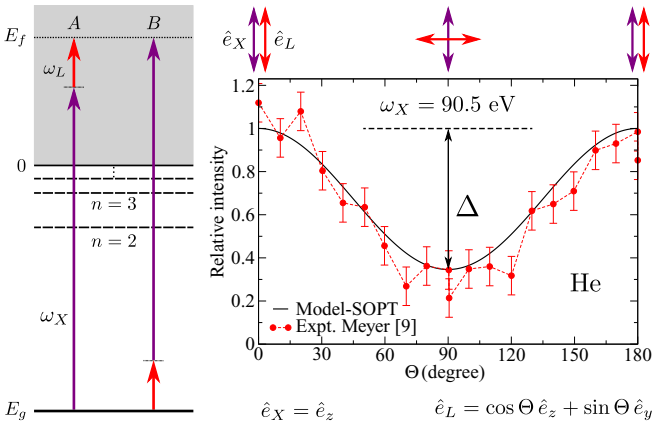

FIG. 1. Left panel: Schematic representation of the two-color two-photon absorption process in helium. Upon absorption of the EUV photon, a bound electron is promoted to a continuum (intermediate) state. The further absorption of a photon from the IR source leaves the photoelectron in its final state, with energy E_f (path A). Additionally, as the EUV and IR sources overlap in time, the time-reversed reaction, accounting for the dressing of the initial state by the IR field (path B), must be taken into account. Right panel: Relative sideband intensity modulation as a function of the relative polarization angle Θ between the fields. The full red dots correspond to previous experimental results [9] (with error bars) and the black full line corresponds to second-order perturbation theory results (see main text).

a dressing field of 523 nm are also plotted (triangle down). The theoretical data corresponding to applying second-order perturbation theory (SOPT) in He taken from [13] are shown with square symbols. We have included our SOPT simulations for H atom, also assuming infinitely long pulses, where the corresponding second-order matrix elements have been evaluated following the formalism given in [14] for hydrogenlike targets. Finally, the sideband modulation predicted by the soft-photon limit is also plotted for the higher energies as a dash-dotted line and labeled in the figure. As expected, it yields a reliable estimation for relatively high photoelectron energies with respect to the frequency of the dressing field.

The sideband intensity modulation monotonically decreases as the EUV photon energy is reduced. Since the algebra associated to the angular degrees of freedom does not depend upon photon energy, the observed smooth variation is necessarily related to the radial matrix elements for the optically allowed final state channels (s and d). In second-order perturbation theory, the total cross section for the two-photon single ionization of an electron initially in an s state can be written as [15]

$$\sigma(\Theta) \propto 3S_2 + (5S_0 + S_2)\cos^2\Theta, \tag{1}$$

where Θ is the relative polarization angle and $S_l = |T_l|^2$ and T_l $(l = 0, 2)$ are the radial matrix elements associated to the emission of an electron in the s and d partial waves, respectively. The above equation provides the link between

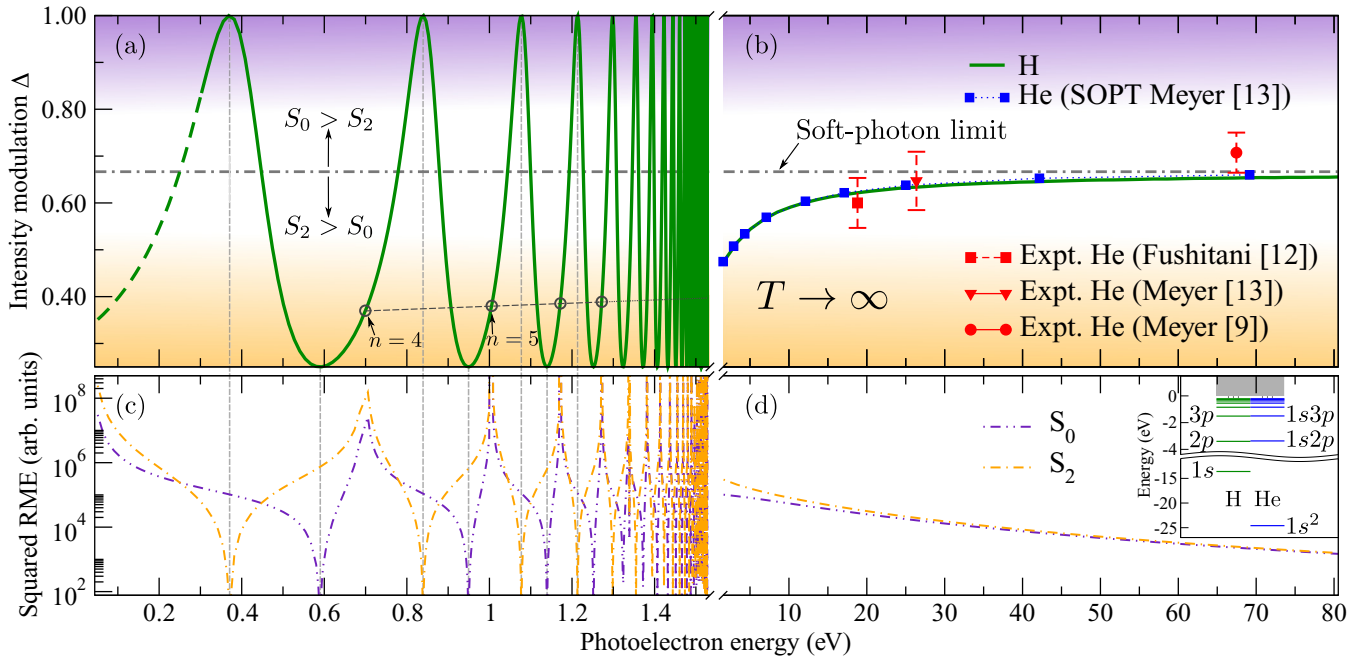

FIG. 2. (a), (b) Intensity modulation (Δ) as a function of the photoelectron energy. Green full line corresponds to the hydrogenlike perturbation theory model explained in the main text, therefore assuming infinitely long pulses ($T \to \infty$). Red filled symbols (squares, triangles, and circles) correspond to experimental data of previous studies shown in the legend. Blue filled squares are the theoretical results extracted for helium from the data presented in Ref. [13]. Orange (lower) shadow region in panels (a) and (b) corresponds to the situation where $S_2 > S_0$. Violet upper shadow region corresponds to $S_0 > S_2$, with S_0 and S_2 being the modulus squared value of the radial matrix elements (RME) associated to emission of an electron in the s and d partial wave, respectively. Vertical dashed thin lines in (a) and (c) indicate the position of the minima for each partial wave. Open circles in panel (a) indicate the energy position of the excited states for the H atom ($n = 4$, $n = 5$, etc.). (c), (d) Modulus squared of the radial partial wave amplitudes as a function of the photoelectron energy. The inset in panel (d) show the energetics in H and He atom. The energy differences between the excited states, as we can see, are very close in energy.

the intensity modulation Δ and the radial matrix elements T_l for each final state channel. Replacing the expressions for $\sigma_{\parallel,\perp}$ obtained through Eq. (1) into the definition of the intensity modulation, we obtain

$$\frac{S_0}{S_2} = \frac{4\Delta - 1}{5(1-\Delta)}. \tag{2}$$

As shown in Fig. 2(d), in the high photoelectron energy limit, the radial probabilities for the s and d partial waves become equal and $\Delta = 2/3$, corresponding to the value obtained in the soft-photon approximation [10]. The results for our second-order perturbation calculations for a hydrogenlike atom (green full line) shown in Fig. 2, panels (a) and (b), converge to this value for high EUV photon energies. As explained in [9], this result shows a failure of the propensity rule [16] that favors the population of partial waves with higher angular momenta. On the other hand, by means of Eq. (2), it can easily be shown that sideband modulation values smaller than $2/3$ necessarily imply that $S_0/S_2 < 1$, in agreement with the propensity rules.

We now retrieve the intensity modulation for low EUV photon energies, lying below threshold, which, to our knowledge, has not been yet investigated in detail and, as we show in the following, is significantly larger than the modulation found in existing ATI experiments. In Fig. 2(a), we show the results for the intensity modulation as a function of the photoelectron energy for the below-threshold ionization process. In contrast with the monotonic variation shown in Fig. 2(b) for the ATI region, where we observe a smooth decrease from $\simeq$0.67 in the asymptotic limit down to 0.47 close to threshold, we now find an oscillatory behavior with the photoelectron energy and a significantly larger intensity modulation, with values varying in the range 0.25 to 1.0. According to Eq. (2), the largest (smallest) values for the oscillation correspond to an electron emission exclusively into the partial waves s (d). The modulus squared of the radial matrix elements for s (S_0) and d (S_2) are shown in Fig. 2(c). In other words, the largest and smallest values of Δ indicate the emission of an electron exclusively associated to a single partial wave, a feature that can be also experimentally accessed by measuring the photoelectron angular distributions [17].

To the best of our knowledge, one experimental study has been reported using such a below-threshold polarization control scheme [18], which was carried out in helium atom. However, the frequency of the pump pulse was tuned to resonantly excite one intermediate $1snp$ bound state of helium, whereas the probe pulse was delayed in time in order to decouple the excitation and ionization processes. Additionally, by varying the relative orientation between the polarization vectors of the fields, the experimental data provide an estimation of the partial cross sections ratio, showing a preferential emission of d electrons. The corresponding value for the intensity modulation can be obtained from the fit to the experimental results from [18] and yields $\Delta = 0.365$, in good agreement with our present results. As it can be seen in Fig. 2(a), the largest degree of polarization control is achieved for EUV frequencies off resonance with transitions to excited states. The empty circles following the thin dashed line in Fig. 2(a) correspond to the theoretical results for the intensity modulation corresponding to EUV photon energies in resonance with intermediate np states in hydrogen ($n = 4,\ n = 5$, etc).

Our result for the $1s - np$ resonant condition gives $\Delta \sim 0.37$, in excellent agreement with the quoted experimental value measured for the $1s2p$ excited state of helium. Note that the on-resonance intensity modulation only shows a slight (linear) increase as the intermediate state is higher, as evidenced in Fig. 2(a) (dashed line with empty circles). There is a very small variation for Δ values corresponding to different resonant intermediate states, which can be indeed expected. For resonant frequencies, one can assume that a single second-order term dominates, $M_{fg}^{(2)} \propto \langle f|D_2|\nu\rangle\langle\nu|D_1|g\rangle$, for each partial wave; therefore, in the definition of Δ, the dependence with $\langle\nu|D_1|g\rangle$ factors out, resulting in a small variation associated to the transition from an excited to a continuum state. In addition, because the IR induced transition from the intermediate excited to the continuum states are expected to be similar for H and He atoms, both in energy [see inset in Fig. 2(d)] and oscillator strength [17], it results in an almost identical intensity modulation. In other words, within the above constraints, the intensity modulation remains qualitatively independent of the target, as long as the active electron has the same principal quantum number and the intermediate and final states are well represented by bound and/or continuum hydrogenic states with charge $Z = 1$.

In Fig. 2(c), we can also see the repeated departure from the propensity rule [16]. The dominance region for each partial wave is delimited by the horizontal dash-dotted line at $\Delta = 2/3$ in Fig. 2(a). At variance with the above-threshold case, where the condition $S_0 \sim S_2$ is obtained only asymptotically, in Fig. 2 we can observe a sequence of photoelectron energy regions with a clear dominance of S_0, as a consequence of interferences between the contributing two-photon amplitudes [19]. In Fig. 3 we show the absolute value for the contributing two-photon amplitudes for hydrogen atom associated to each intermediate state, as indicated in the legends and plotted as a function of the final photoelectron energies. The upper panel shows the terms that contribute to the final s partial wave, while the bottom panel correspond to the d wave. As it is known, there is a change of sign at the resonant energy with each transition (dashed lines indicate a negative value of the amplitude and lines with star symbols correspond to positive values). The vertical dashed lines in the plots indicate an almost zero value for the resulting s (or d) amplitude.

For instance, for the s partial wave (top panel of Fig. 3), the position of the minima is governed mainly by two contributions. One of them corresponds to the nearest excited intermediate state, with higher energy. This contribution has a negative value. The second contribution is the one associated to the integral over the continuum spectrum of the atom. This contribution will be always positive. The minima in the d partial wave however are mostly the result of cancellations between two-photon path contributions from consecutive resonant bound states, as discussed in a recent theoretical study of photoelectron angular dichroism in two-photon atomic ionization [20]. The continuum contribution in the d partial wave is only expected to play a role for the higher lying Rydberg states.

It should be also noted that the observation of this strong oscillatory behavior in the intensity signal requires the

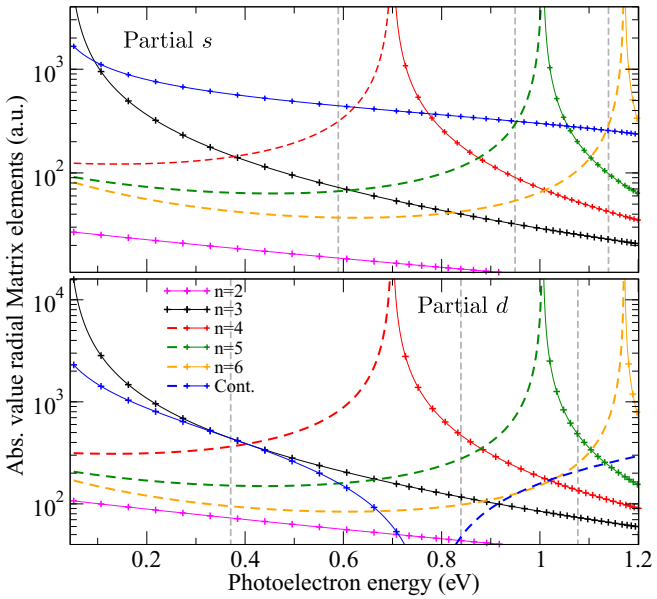

FIG. 3. Absolute value of (radial) transition matrix elements corresponding to individual intermediate bound states, and continuum states for a hydrogenlike atom. For clarity purposes, we indicate positive values by thin lines and plus symbols. Negative values are indicated by the dashed lines of the same color. The vertical dashed lines indicate position of the resulting minima shown in Fig. 2(c).

availability of tunable EUV frequencies, but also relatively long pulses such that there is a larger contribution of specific two-photon paths; otherwise, we rapidly enter in the dominance of the ATI continuum. Figure 4 shows results of second-order time-dependent perturbation theory for different pulse durations of both the EUV and the IR fields (both are assumed to have the same pulse duration). It can be seen that the interaction with an ultrashort laser pulse washes out the oscillations enclosed by higher lying Rydberg intermediate states. However, the first and second maxima obtained for infinitely long pulses are still visible even for a 7 fs pulse. Additionally, as the branching ratio can also be obtained from measurements of the angular distributions in two-photon single ionization, starting from Eq. (2) we can estimate the intensity modulation from those measurements. In particular, we have extracted the intensity modulation from the experimental data of Mondal *et al.* in Ref. [21]. Those measurements correspond to the ionization of resonantly excited helium states. In that case, the authors found that the coherence time was 7 fs and, therefore, the experimental results should be compared with our theoretical estimation for that duration of the pulses. It can be seen that our simple model is able to reproduce the experimental results within the error bars, except for the $1s5p$ state, where a slight deviation is observed. Similar agreement is found with other measurements [22]. Note the good agreement with the experiment, retrieving the same trend as that shown for infinitely long pulses and plotted in Fig. 2(a) in dashed line.

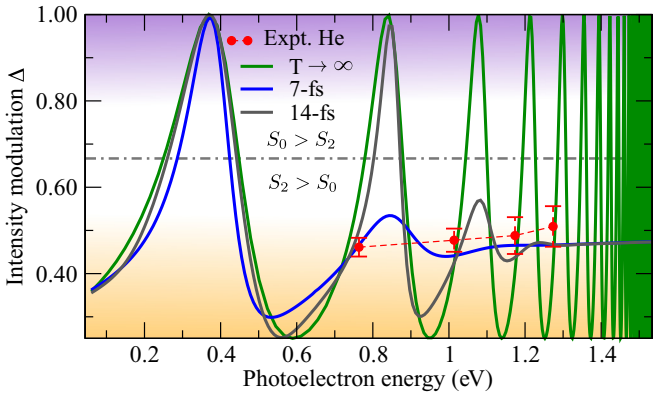

FIG. 4. Intensity modulation Δ as a function of the photoelectron energy, for different pulse durations of both the EUV and the IR dressing fields. Symbols with error bars correspond to the experimental data from [21].

To summarize, we have shown the higher degree of control that can be achieved by manipulating the light polarization between pulses in two-color atomic photoionization below threshold. We have presented second-order time-independent and time-dependent perturbation theory results showing that by scanning the EUV photon energy in the presence of an IR dressing field it is possible to control the relative ionization yields with respect to the angle between the fields. Besides the results shown here for hydrogenlike atoms, we have further checked that lithiumlike targets would show a much more spiked oscillation pattern due to the dominance of intrashell $2s - 2p$ transitions over the background continua. In such a case, the minima for s and d partial waves will be located much closer to each other. It should be stressed that these effects are expected to be not solely restricted to ionization of electrons associated to s orbitals. As shown in the present manuscript, the sequence of minima in the partial cross sections resulting by contributing neighbor resonances due to bound excited intermediate states are encountered in almost every atomic and molecular target. Therefore, analogous control schemes, as this one proposed for hydrogen and helium targets, are expected to also be achievable in larger multielectronic systems.

We acknowledge support from the Ministerio de Economía y Competitividad, through Projects No. FIS2016-77889-R and No. FIS2017-92382-EXP, and through the Ramón y Cajal contract from AP. D.B. and O.F. acknowledge financial support from Agencia Nacional de Promoción Científica y Tecnológica, Project No. PICT 2015-3392, and No. PIP 0784 from Consejo Nacional de Investigaciones Científicas y Técnicas, from República Argentina. Simulations were performed with computer time allocated at MareNostrum at Barcelona Supercomputing Center (BSC) through the Spanish Supercomputing Network (RES) and in the Centro de Computación Científica at UAM.

[1] C. Bostedt, H. N. Chapman, J. T. Costello, J. R. Crespo López-Urrutia, S. Düsterer, S. W. Epp, J. Feldhaus, A. Föhlisch, M. Meyer, and T. Möller, Nucl. Instrum. Methods, Phys. Res. A **601**, 108 (2009).

[2] F. Holzmeier, R. Y. Bello, M. Hervé, A. Achner, T. M. Baumann, M. Meyer, P. Finetti, M. Di Fraia, D. Gauthier, E. Roussel, O. Plekan, R. Richter, K. C. Prince, C. Callegari, H. Bachau, A. Palacios, F. Martín, and D. Dowek, Phys. Rev. Lett. **121**, 103002 (2018).

[3] M. Meyer, J. T. Costello, S. Düsterer, W. B. Li, and P. Radcliffe, J. Phys. B **43**, 194006 (2010).

[4] K. C. Prince, E. Allaria, C. Callegari, R. Cucini, G. De Ninno, S. Di Mitri, B. Diviacco, E. Ferrari, P. Finetti, D. Gauthier, L. Giannessi, N. Mahne, G. Penco, O. Plekan, L. Raimondi, P. Rebernik, E. Roussel, C. Svetina, M. Trovò, M. Zangrando *et al.*, Nat. Photon. **10**, 176 (2016).

[5] L. Giannessi, E. Allaria, K. C. Prince, C. Callegari, G. Sansone, K. Ueda, T. Morishita, C. N. Liu, A. N. Grum-Grzhimailo, E. V. Gryzlova, N. Douguet, and K. Bartschat, Sci. Rep. **8**, 7774 (2018).

[6] A. K. Kazansky, A. V. Grigorieva, and N. M. Kabachnik, Phys. Rev. A **85**, 053409 (2012).

[7] F. J. Wuilleumier and M. Meyer, J. Phys. B **39**, R425 (2006).

[8] A. A. Lutman, J. P. MacArthur, M. Ilchen, A. O. Lindahl, J. Buck, R. N. Coffee, G. L. Dakovski, L. Dammann, Y. Ding, H. A. Dürr, L. Glaser, J. Grünert, G. Hartmann, N. Hartmann, D. Higley, K. Hirsch, Y. I. Levashov, A. Marinelli, T. Maxwell, A. Mitra *et al.*, Nat. Photon. **10**, 468 (2016).

[9] M. Meyer, D. Cubaynes, D. Glijer, J. Dardis, P. Hayden, P. Hough, V. Richardson, E. T. Kennedy, J. T. Costello, P. Radcliffe, S. Düsterer, A. Azima, W. B. Li, H. Redlin, J. Feldhaus, R. Taïeb, A. Maquet, A. N. Grum-Grzhimailo, E. V. Gryzlova, and S. I. Strakhova, Phys. Rev. Lett. **101**, 193002 (2008).

[10] A. Maquet and R. Taïeb, J. Mod. Opt. **54**, 1847 (2007).

[11] T. Leitner, R. Taïeb, M. Meyer, and P. Wernet, Phys. Rev. A **91**, 063411 (2015).

[12] M. Fushitani, A. Matsuda, and A. Hishikawa, J. Electron Spectrosc. Relat. Phenom. **184**, 561 (2012).

[13] M. Meyer, D. Cubaynes, J. Dardis, P. Hayden, P. Hough, V. Richardson, E. Kennedy, J. Costello, S. Düsterer, W. Li, P. Radcliffe, H. Redlin, J. Feldhaus, S. Strakhova, E. Gryzlova, A. Grum-Grzhimailo, R. Taïeb, and A. Maquet, J. Electron Spectrosc. Relat. Phenom. **181**, 111 (2010).

[14] V. Véniard and B. Piraux, Phys. Rev. A **41**, 4019 (1990).

[15] R. Taïeb, V. Véniard, A. Maquet, N. Manakov, and S. Marmo, Phys. Rev. A **62**, 013402 (2000).

[16] U. Fano, Phys. Rev. A **32**, 617 (1985).

[17] D. I. R. Boll, O. A. Fojón, C. W. McCurdy, and A. Palacios, Phys. Rev. A **99**, 023416 (2019).

[18] A. Johansson, M. K. Raarup, Z. S. Li, V. Lokhnygin, D. Descamps, C. Lyngå, E. Mevel, J. Larsson, C.-G. Wahlström, S. Aloise, M. Gisselbrecht, M. Meyer, and A. L'Huillier, Eur. Phys. J. D **22**, 3 (2003).

[19] F. H. Faisal, *Theory of Multiphoton Processes*, 1st ed. (Springer US, New York, 1987).

[20] J. Hofbrucker, A. V. Volotka, and S. Fritzsche, Phys. Rev. Lett. **121**, 053401 (2018).

[21] S. Mondal, H. Fukuzawa, K. Motomura, T. Tachibana, K. Nagaya, T. Sakai, K. Matsunami, S. Yase, M. Yao, S. Wada, H. Hayashita, N. Saito, C. Callegari, K. C. Prince, P. O'Keeffe, P. Bolognesi, L. Avaldi, C. Miron, M. Nagasono, T. Togashi *et al.*, J. Phys. B **46**, 205601 (2013).

[22] P. O'Keeffe, A. Mihelič, P. Bolognesi, M. Žitnik, A. Moise, R. Richter, and L. Avaldi, New J. Phys. **15**, 013023 (2013).